WILEY

Magnetic resonance imaging image analysis of the therapeutic effect and neuroprotective effect of deep brain stimulation in Parkinson's disease based on a deep learning algorithm

Jianzhong Zhang[1] | Chaoyang Zhou[1] | Xiang Xiao[1] | Weihua Chen[2] | Yi Jiang[3] | Ronglan Zhu[1] | Tao Xin[1]

[1]Department of Neurosurgery, The First Affiliated Hospital of Nanchang Medical College, Nanchang, China

[2]Department of Imaging, The First Affiliated Hospital of Nanchang Medical College, Nanchang, China

[3]Network Information Center, The First Affiliated Hospital of Nanchang Medical College, Nanchang, China

Correspondence
Tao Xin, Department of Neurosurgery, The First Affiliated Hospital of Nanchang Medical College, Nanchang 330006, China.
Email: drxintao@126.com

Abstract

In order to study the therapeutic neuroprotective effect of deep brain stimulation (DBS) in Parkinson's disease (PD), based on the deep learning algorithm, this study combines with magnetic resonance imaging (MRI) image analysis technology to study the clinical efficacy of DBS in the surgical treatment of PD and the neuroprotective and neurological recovery effects after surgery. Establish a deep learning algorithm model based on MRI image analysis technology, comparison of UPDRS motor status assessment and the improvement of daily life ability before and after DBS surgery, evaluate the accuracy rate and the detection speed of the model. The models constructed in this study have an accuracy rate of more than 90% in the PD detection test, and the detection speed of the algorithm model under the condition of big data is between 60 and 200 ms. DBS significantly improve a series of clinical symptoms in patients with PD. The deep learning algorithm model based on MRI image analysis technology in this paper has a certain effect. DBS operation can improve the symptoms of PD, and has the effect of neuroprotection and neurological recovery.

KEYWORDS

DBS efficacy, deep learning, magnetic resonance imaging, neuroprotection, Parkinson's disease

1 | BACKGROUND AND OBJECTIVE

1.1 | Parkinson's disease treatment status

Parkinson's disease (PD) is a common and progressively disabling neurodegenerative disease of the nervous system. Its prevalence occurs in middle-aged and elderly people, and the prevalence rate of people over 65 years old in China is as high as 1700/100,000. The clinical features of PD include typical motor symptoms such as bradykinesia, resting tremor,

or muscle rigidity and various non-motor symptoms such as hyposmia, sleep disturbance, constipation, anxiety, and depression.[1]

Although PD cannot be completely cured at present, it is necessary to better treat symptomatically in patients with advanced PD, control motor symptoms, improve non-motor symptoms and motor complications, and improve the quality of life of patients.[2] Deep brain stimulation (DBS) is a surgical treatment for patients with advanced PD who are not sensitive to drug control. The mechanism is mainly to use microelectrodes to stimulate the deep brain motion control nucleus with high frequency to simulate damage,[3] thereby controlling symptoms. Because of its adjustability and low incidence of complications, it is widely used. The ventra intermediate nucleus (Vim) and the medial nucleus of the globus pallidus (Gpi) have been used as targets for surgical treatment. Because the subthalamic nucleus (STN) can relatively comprehensively control the motor symptoms of PD, it is currently the most commonly used target for the treatment of PD. The advantage of DBS of the subthalamic nucleus (STN-DBS) over drug therapy is the relatively continuous control of symptoms and reduction of motor complications. In addition, dopaminergic drugs often cause mental symptoms such as hallucinations and motor complications, which limit medical treatment. However, STN-DBS can significantly reduce the amount of levodopa, thereby reducing the occurrence of adverse drug reactions and improving the quality of life of patients. Although most studies at home and abroad lack randomized controls, and long-term (more than 10 years) efficacy data is still in the accumulation stage, many studies have been published to confirm the safety and effectiveness of surgical treatment of suitable patients (Table 1).

Deep brain stimulation uses electrodes implanted in the brain to send electrical discharge pulses to the relevant nerve nucleus that controls movement to regulate abnormal nerve electrical activity, so as to achieve the purpose of reducing and/or controlling symptoms. Moreover, it is currently one of the most effective and safest treatments for primary PD, idiopathic tremor and dystonia. DBS was first used in the treatment of intractable pain in the 1950s and later in the treatment of epilepsy. In 1984 Tasker applied it to clinical treatment of PD. Since Benabid and others began to use DBS to stimulate the ventrolateral thalamic nucleus in the treatment of PD tremor and idiopathic tremor, DBS has developed rapidly and has gradually replaced traditional destructive surgery. China began to implement DBS surgery in 1998 and achieved good treatment results. The DBS system includes an electrode implanted in the brain and a pulse generator implanted in the body. The currently used electrode is a four-contact electrode connected to the pulse generator implanted under the skin. The pulse generator can be adjusted by an external controller to deliver different types of electrical stimulation. The carbon-lithium battery can last for several years, and the service life depends mainly on the level of the selected stimulation parameter. The stimulation parameters can be adjusted according to the selected stimulation mode (single-stage or bipolar) and stimulation contacts.[4]

At present, the international clinical evaluation of PD is mostly based on the unified Parkinson′s disease rating scale (UPDRs), which mainly evaluates the exercise status and daily living ability of PD patients. Although the results of different research centers are different, the effects are positive. In this article, we will follow up the patients with PD who have undergone DBS surgery and are programmed in our center to evaluate the treatment effect.

1.2 | The concept of reinforcement learning

Reinforcement learning (RL) is a special machine learning method that maps from state to action. Its goal is to enable the agent to obtain the largest cumulative reward in the interaction with the environment. Agent refers to a computing

TABLE 1 Comparison of UPDRS III score and UPDRS II score.

Point in time	status	n	UPDRS III	UPDRS II
Preoperative	Not taking medicine	10	44.7 ± 3.8	32.8 ± 5.7
	Taking medicine	10	19.4 ± 1.6 (56.7%)	11.6 ± 4.6 (64.6%)
6 months after operation	Not taking medicine + not turn on	10	45.5 ± 4.4	33.2 ± 5.2
	Not taking medicine + booting	10	20.4 ± 1.7 (55.4%)	12.4 ± 4.2 (62.7%)
	Take medicine + boot	10	18.7 ± 1.1 (58%)	10.5 ± 4.1 (69.4%)
12 months after operation	Not taking medicine + not turn on	10	45.7 ± 4.4	33.8 ± 5.7
	Not taking medicine + booting	10	20.5 ± 1.7 (54.5%)	12.2 + 4.4 (63.5%)
	Take medicine + boot	10	18.7 ± 1.0 (58%)	10.4 ± 4.5 (68.3%)

entity that can stay in a state of a certain environment and can continuously play its role and function. In RL, it refers to an entity that runs a RL algorithm. What is considered in RL is a holistic problem, which is a problem of the interaction between the goal-oriented Agent and the unknown environment. In general, unlike other machine learning problems, it cannot be split into many sub-problems to solve. In the process of RL, the reverse solution is adopted, which is an interactive target search solution.

Reinforcement learning is widely used and is considered to be a core technology towards general artificial intelligence. It has decision-making and control functions and is often used in games. The control and decision-making problems involved can be abstracted into RL models. Similar to other machine learning problems, RL also has a training process, which needs to continuously perform actions, and observe the results after performing actions, and form an RL model by continuously accumulating experience. Unlike traditional learning, each action generally has no directly calibrated label value as supervisory information, and the system only gives the algorithm a feedback after performing the action. The result of the current action will be fully reflected in the future, that is, the feedback is delayed. Agent needs to observe the environment and its own state information, and then perform the corresponding actions to achieve the desired result. The schematic diagram of the RL model is shown in Figure 1.[5]

In summary, as an action entity of RL, Agent has its own state at every moment, and the surrounding environment, and Agent can determine the corresponding action according to the current state and execute the action. After that, the agent and the environment will enter the next state space, and at the same time, the system will give it a feedback value to reward or punish the actions performed so that the Agent can perform the desired actions.

1.3 | The model of the RL problem

Usually, Markov decision process (MDP) can be used to model the RL problem. The characteristic of MDP is that the state of the system at the next time has nothing to do with the earlier time and is only determined by the state at the current time. MDP can be expressed as a quadruple (S, A, ρ, f). Among them[6]:

S is the set of environmental states, and $s_t \in S$ represents the state of the agent at time t;

A is the set of actions performed by the Agent, and $a_t \in A$ represents the actions performed by the Agent at time t;

$\rho : S \times A \rightarrow R$ is the reward function, and $r_t \sim \rho(s_t, a_t)$ represents the instant reward value obtained by the Agent at time t, when the environment state is s_t and the action is a_t;

$f : S \times A \times S \rightarrow [0, 1]$ is the state transition probability distribution function, and $s_{t+1} \sim f(s_t, a_t)$ is the probability that the Agent will transition to the next state s_{t+1} when the action is a_t and the environment state is s_t.

In the RL problem, strategy $\pi : S \rightarrow A$ represents the mapping of state to action. In state s_t, the probability that Agent selects a_t in action set A and executes the action and transitions to the next state s_{t+1} is $f(s_t, a_t)$. At the same time, Agent will also receive instant rewards r_t from environmental feedback. Usually, a discount factor γ is used to weigh the effect of future rewards on the cumulative rewards, where $\gamma \in (0, 1)$. From the beginning of time t to the end of time T, the cumulative reward can be expressed as:
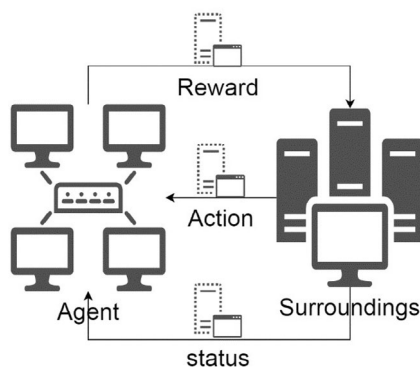

FIGURE 1   Reinforcement learning model

$$R_t = \sum_{t'=t}^{T} \gamma^{t'-t} r_{t'} \tag{1}$$

In the RL problem, a value function $V^\pi(s, a)$ is introduced, which means that in the current states, the Agent performs action a and executes the entire process in accordance with strategy π until the end of the RL algorithm. The cumulative return obtained during this process can be expressed as:

$$V^\pi(s, a) = E[R_t | s_t = s, a_t = a, \pi] \tag{2}$$

The value function represents the expectation of the cumulative rewards obtained by the agent executes the entire process according to strategy π when the state is s and the execution action is a, which is characterized by the cumulative return of strategy π.[7]

In the RL process, each state corresponds to each action. Therefore, if there are several state action pairs, for these state action pairs, if the cumulative return of strategy π^* is not less than the cumulative return of other strategies, then strategy π^* is called the optimal strategy. In the actual RL problem, there may be multiple optimal strategies, and different optimal strategies follow the same value function:

$$V^*(s, a) = \max_\pi E[R_t | s_t = s, a_t = a, \pi] \tag{3}$$

The above formula is called the optimal value function, and the optimal value function can be given in the form of the Bellman equation:

$$V^*(s, a) = E_{s' \sim S}[r + \gamma \max_{a'} V(s', a') | s, a] \tag{4}$$

The above formula is the Bellman equation, which expresses the relationship between the value function of the current state and the value function of the next state. It can be known from the Bellman equation that the solution process of the value function is an iterative calculation process of dynamic programming. In the traditional RL problem, the value function is usually solved by iterating the Bellman equation:

$$V_{i+1}(s, a) = E_{s' \sim S}[r + \gamma \max_{a'} V_i(s', a') | s, a] \tag{5}$$

When $i \to \infty$, $V_i \to V^*$, that is, through continuous iterative calculation, the value function will eventually converge to obtain the optimal strategy: $\pi^* = \arg\max_{a \in A} V^*(s, a)$. However, in the actual RL task, because the state set is particularly large, the calculation scale and cost of the iterative calculation method are very large. Therefore, iteratively solving the optimal strategy is unrealistic. To solve this problem, in the specific RL algorithm, various linear functions can be used to approximate the value function with arbitrary precision, that is, $V(s, a) \approx V^*(s, a)$.[8] In addition, a neural network can be used to design a function approximator to approximate the value function.

1.4 | The limitations and goal of the reinforcement learning algorithm

The RL algorithm introduced above has many limitations in specific applications.[6–8] The algorithm can only be applied when the state space set and action space set are finite discrete sets. Moreover, the algorithm only works well when the number of state sets and action sets is small, and the state and actions in the RL algorithm need to be designed manually. However, the actual application scenarios are generally more complex, and the state space set is larger, so it is very difficult to define discrete states for specific RL problems. The input data of practical application problems are all high-dimensional, such as images or sounds, so the use of general algorithms requires huge iterative calculation operations, which is obviously unrealistic. In the process of running the algorithm, we can consider using a neural network to fit the value function to avoid a large number of iterative calculation operations. With the emergence of deep learning and great success, it is a natural idea to combine deep neural networks with RL. This is the origin of the basic idea of deep reinforcement learning (DRL). Deep neural networks can achieve end-to-end learning, and directly learn useful

features from high-dimensional input data such as images or sounds, which are more general than artificial design features.[9]

The excellent performance of DRL benefits from the perception ability of deep learning and the decision-making ability of RL. Google's DeepMind team combined the two to propose a deep Q-Network (DQN) model. This model enables Agent to learn a complete set of decision-making system only by observing the pre-processed game image, and even shows the level of surpassing human top players in many games, which is pioneering in the field of DRL. DQN combines CNN and Q learning algorithms and is the first successful DRL algorithm with generality. Next, we introduce Q learning algorithm and DQN algorithm, respectively, as well as some improved algorithms generated on this basis.

The Q-Learning algorithm is the foundation of DQN. The basic idea is to randomly perform different actions through a certain strategy and improve it based on the observed returns. Compared to MDP's model learning algorithm, Q-Learning is a model-free learning algorithm.

The goal of the Q-Learning algorithm is to estimate the maximum value of the action value function to determine the optimal strategy π^*, which reflects the idea of value iteration. A function $Q(s, a)$ is defined in the entire algorithm, which represents the state-action value Q function when the state is s and the agent takes action a. At the beginning of the algorithm, $Q(s, a)$ in the non-terminated state can be initialized to any value, and $Q(s, a)$ in the terminated state needs to be initialized to 0. Then, all the fragments are looped. During the entire cycle, the following operations are performed[10]:

1. The greedy algorithm is adopted, and the corresponding action a is taken under the states according to the Q function;
2. The action a is executed, and the immediate return R and the next state s' are obtained;
3. The state-action value Q function is updated:

$$Q(s, a) = Q(s, a) + \alpha[R + \gamma \max_{a'} Q_i(s', a') - Q(s, a)] \tag{6}$$

Among them, α is the learning rate set manually.

4. The action enters the next state $s = s'$ until it enters the termination state

When taking action "a" in step 2, we can combine exploration and utilization. Exploration is to choose an action at random, while utilization is to choose the most valuable action to be executed by the current action function value:

$$a = \max_{a'} Q(s, a') \tag{7}$$

The optimal action is executed with the probability of ε, and the other actions are executed with the probability of $1 - \varepsilon$. This is the greedy algorithm of $\varepsilon-$. Next, the action enters the next state $s = s'$, and finally converges to the optimal value m of the Q function to obtain the optimal strategy.

DQN cleverly combines CNN and Q-Learning algorithms. Because the way of training the network is very similar to the Q-Learning algorithm, the process of DQN training the network is called Deep Q-Learning. The core of the DeepQ-Learning algorithm is DQN. How to use DQN to guide Agents to make actions and how to optimize the network are the first issues to be considered. DQN is actually a deep CNN structure. The structure of the network is shown in Figure 2.[11]

As shown in Figure 2, the input to the network is a pre-processed 4-frame game image, and the size of the game image is adjusted to 84 × 84. The next step of the model is three convolutional layers. The first convolution layer contains 32 convolution kernels, the size of the convolution kernel is 8 × 8, and ReLU is selected as the activation function for nonlinear processing. The second convolution layer has 64 convolution kernels, the size of the convolution kernel is 4 × 4, and the corresponding activation function is also ReLU. The third convolutional layer is composed of 64 convolution kernels of size 3 × 3. After the nonlinear processing of ReLU, the data stream enters the fully connected layer, which is composed of 512 neurons. Then, there is the output layer. The number of neurons in the output layer corresponds to the number of actions performed in the game. Finally, the output layer outputs the evaluation of the network for each action generated by the current state, that is, the Q value of each action. The network obtains the visual signal to output the value function of the action and executes the action according to the $\varepsilon-$ greedy algorithm.
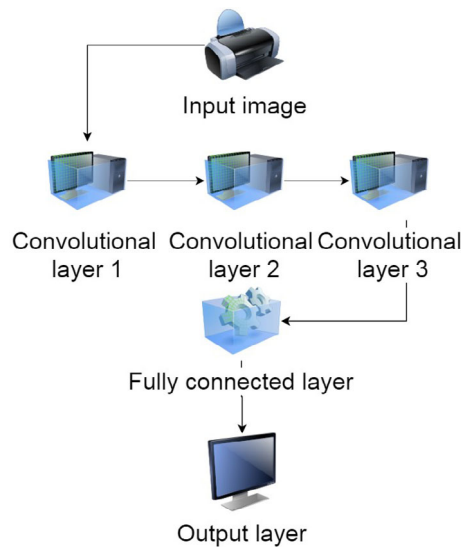
FIGURE 2 DQN model structure

The network structure of the DQN model is no different from the traditional convolutional network. In the field of supervised learning, it can use the labeled data set for network training, but there is no labeled data set in the field of RL. Therefore, how to obtain training samples and design a loss function is a problem to be considered. Inspired by the updated Q value in the traditional RL Q-Learning algorithm, the loss function can be constructed by the output value of the neural network and the updated value of the Q-Learning algorithm[12]:

$$L(\theta) = E\left\{ [R + \gamma \max_{a'}(s', a', \theta) - Q(s, a, \theta)]^2 \right\} \tag{8}$$

In the formula, θ is the parameter of the network. The difference between the output value of the network and the estimated value of the Q function is measured by the Euclidean distance, and the extreme value of the loss function means that the network makes a correct estimate of the current state and obtains the optimal solution.

For the problem of how to obtain training samples, agents can perform actions to generate samples. Current neural networks are used to make predictions and obtain value functions for all actions. Next, according to the strategy, the selected action is executed to obtain a new state and reward value as a training sample. The neural network requires that the training samples are independent of each other, and there is correlation between the samples before and after the game. In order to solve the problems of correlation between training samples and the probability distribution of the training samples is not fixed, DQN uses an experience playback mechanism. During implementation, the samples are first stored in a set, which is called the experience pool. When training the network, random sampling is used to obtain the samples required for each iteration, so as to break the correlation between the original samples.

DQN can achieve end-to-end training and learning without artificially designing features, and it integrates deep learning and RL. Moreover, when solving various tasks based on visual perception, it can adopt similar network models, optimization training methods and parameter configuration methods. These advantages fully illustrate the versatility of DQN.

For the DQN algorithm, in the process of optimizing the objective function, each operation selects the action with the largest Q value in the new state. The action of selecting and evaluating is generally through the parameter θ of the neural network. This operation will lead to the problem of overestimating the Q value during the RL process. In response to this problem, some improved algorithms have emerged, and Hasselt et al. proposed the Deep Double Q-Network (DDQN) algorithm. There are two different parameters in this algorithm: θ and θ^-. Among them, θ to select the action under the maximum Q value, θ^- to evaluate the Q value under the optimal action conditions. The action and evaluation strategy can be selected through the two parameters, which reduces the risk of overestimation of the Q value to a certain extent.

Although the experience playback mechanism can solve the problem of correlation between samples, this mechanism also has some limitations. First, the Agent consumes a lot of memory resources during the interaction with the state of the environment and requires a certain amount of computing power. Second, the experience playback mechanism requires the Agent to adopt the off-strategy method, which will cause delays in updating the strategy. In response to the above problems, Mnih et al. proposed the idea of asynchronous RL and further applied it in the field of DRL, which produced a lightweight DRL framework.[13] This framework can use asynchronous gradient descent to optimize network parameters. Among them, the Asynchronous Advantage Actor-Critic (A3C) algorithm has better performance. The algorithm uses multiple threads to execute multiple agents in parallel and asynchronously. Parallel agents can be in different states respectively, which solves the correlation of samples and can replace the experience playback mechanism to a certain extent. At the same time, the algorithm also reduces the requirements for computer hardware, and only requires a multi-core CPU to execute. It is a low-cost DRL algorithm, so it has gradually become the most common DRL algorithm.

2 | METHODS

2.1 | The role of implementation principle of image cropping model

On the one hand, the image cropping operation can improve the composition of the original image, and it can also be used as an effective work to extract key features of the image. In this paper, the entire image cropping is regarded as a Markov sequence decision-making process, so that the idea of RL is introduced into the entire process. By constructing the cropping environment, the agent is interacted with it, and the corresponding actions are taken from the defined action space to optimize the target to complete the cropping operation, so as to achieve the purpose of extracting the effective information of the image. In the RL environment, the input image and the crop window are used as state observations, and a series of actions that the Agent may take are defined. The agent takes corresponding actions from the action set according to the state observation to perform cropping operations on the image, and fine-tunes the shape and position of the cropping window. After the current action is executed, the agent receives a reward according to the reward function of the cropped image, accumulates each reward and maximizes it, and continuously performs the image cropping operation, thereby outputting the best cropped image as the distinctive feature part of the image.

2.2 | How to realize the implementation principle of the image cropping model

Firstly, the action set needs to be set during the image cropping process. Which action to take is the specific manifestation form of the Agent's decision-making role. For image cropping, commonly used actions include zooming (a), position conversion (b), and aspect ratio conversion (c). Agents can adjust the size and shape of the cropping window by performing these three sets of actions. The set of actions for specific settings is shown in Figure 3.

In addition, a special termination action is also set in the common action set. The termination action exists independently as a trigger. Once this action is selected, the Agent stops the image cropping operation and uses the cropped image obtained by it as the final output result. In addition, during the execution of each action, through multiple trial and error, the zoom factor is set to .55, that is, the size of the cropped sub-window is .55 times the original image. By reasonably setting the scaling factor, the most relevant area of the image and its characteristics can be effectively extracted to represent the entire image. This area depicts the overall shape and structural characteristics of the target information. At the same time, the position, size and aspect ratio of the crop window can be adjusted more accurately, so that the characteristic content of the most relevant area is more complete, so that the accuracy of the crop window capture can be improved to a certain extent, and a more accurate crop image can be obtained. In this way, the non-feature information in the image is excluded, which is reasonable.

In the process of image cropping based on RL, it is necessary to define the current cropping environment state, which provides detailed observation information, so that the Agent can play a decision-making role. $s_t \in S$ represents the state of the Agent at time t, and its corresponding current observation can be expressed as O_t. In the process of image cropping, the state before t and its observations also have a certain influence on the final cropping result, so

(A) Zooming

(B) Position conversion

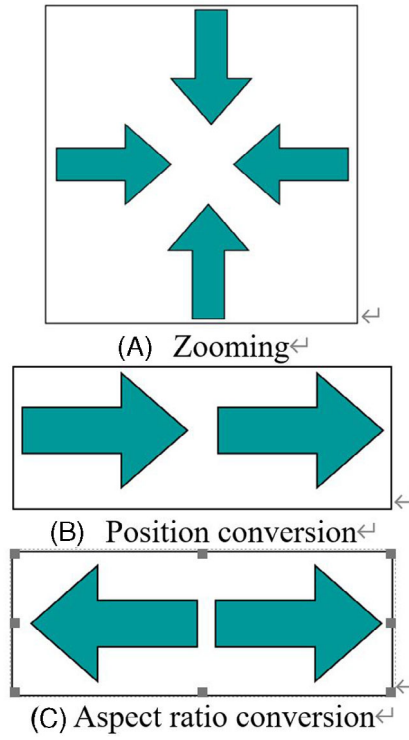(C) Aspect ratio conversion

FIGURE 3 Defined common action set

historical observations before t also need to be considered. Historical observations can be expressed as $\{O_0, O_1, \cdots, O_{t-1}\}$. The state S_t is a combination of the two and can be expressed as:

$$S_t = \{O_0, O_1, \cdots, O_{t-1}, O_t\} \tag{9}$$

In the implementation process of specific image cropping, a long-short-term memory network (LSTM) with memory function is used to memorize and store historical observations. The current observation value O_t consists of the crop window and the characteristics of the input image.

Similar to the traditional RL problem, the image cropping model with RL as its thought also needs to set a reward function. The reward function can measure the reward of the agent for performing relevant actions during the image cropping process and can also guide the agent to continuously optimize the actions during the image cropping process to obtain the most characteristic image. Generally speaking, the most characteristic part of an image is the image saliency area. The saliency area reflects the degree of interest of human vision in this part of the area. The original image and its saliency area are shown in Figure 4.

As can be seen from the above figure, the saliency area better describes the target object in the image and embodies good visual characteristics. In theory, the overall area of the cropped image changes continuously throughout the process, so the difference between the area of the significant area and the area of the cropped image can be used to characterize the reward function Reward, namely:

$$Reward = \frac{area(S_{t+1})}{area(I_{t+1})} - \frac{area(S_t)}{area(I_t)} \tag{10}$$

Among them, $area(I_t)$ and $area(S_t)$ area represents the area of the cropped image and the area of the salient region of the corresponding cropped image during the t-th execution process. To simplify the representation, we set:

$$P_t = \frac{area(S_t)}{area(I_t)} \tag{11}$$

Therefore, the above formula can be expressed as:

(A) The original image
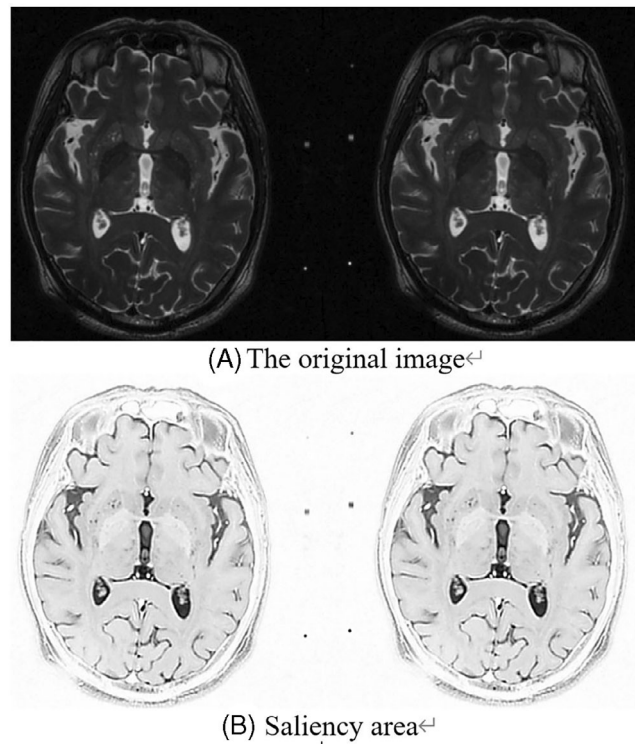

(B) Saliency area

FIGURE 4 Original image and saliency area (3.0 T MRI)

$$Reward = P_{t+1} - P_t \tag{12}$$

when the difference is positive, it means that the Agent gets a positive reward, otherwise the agent gets a negative reward. In addition, in order to ensure that the cutting process requires fewer iteration steps and to accelerate the entire cutting process, additional negative rewards are added. The negative reward coefficient is .01. At the same time, we use the sign function $sign(\cdot)$ to limit its output to $[-1, 1]$, to ensure the stability and convergence of the training process. Therefore, in the cutting process, the reward function can be defined as:

$$r_t = sign(P_{t+1} - P_t) - 0.01 \times (t+1) \tag{13}$$

Among them, $t+1$ is the number of steps taken by the Agent from the start of the action.

There are many related algorithm models for image salient region detection. In this paper, based on the principle of simplicity and efficiency, the spectral residual (SR) model is used as the saliency region calculation method.[14] The model is simple to operate, has nothing to do with features, and has high universality. The following focuses on the core idea of the method.

The model analyzes the image from the perspective of information theory, finds that there is a certain relationship between the image saliency area and the image log spectrum in the image space frequency domain, and calculates the image saliency area by defining the remaining spectrum $R(f)$. First, the model performs Fourier transform on the image to obtain the amplitude spectrum and phase spectrum of the image, respectively:

$$A(f) = R[F(I(x))], P(f) = S[F(I(x))] \tag{14}$$

Then, the model turns the amplitude spectrum into a log spectrum by taking the logarithm:

$$L(f) = \log[A(f)] \tag{15}$$

Then, the model will perform spatial filtering on the log spectrum (using 3×3-means filtering) and make a difference between the two to get the remaining spectrum:

$$R(f) = L(f) - h_n(f) * L(f) \tag{16}$$

Finally, the model performs inverse Fourier transform through the residual spectrum and the phase spectrum, and then filters through the Gaussian filter to obtain a saliency map:

$$S(x) = g(x) * F^{-1}\{\exp[R(f) + P(f)]\} \tag{17}$$

Because the SR model is simple to execute, has high efficiency, has nothing to do with the specific characteristics and types of the image, and has a wide applicability, it is used as a calculation method for the saliency region of the cropped image in the reward function. Therefore, it is feasible to use the SR model to process the magnetic resonance imaging (MRI) data of patients with PD, and the calculation method of cropping the salient area of the image is feasible.

2.3 | Image cropping model structure

The structure of the entire model is shown in Figure 5. First, the cropped image generated during the first forward propagation process is extracted by a convolution structure (Conv), which is called a local feature, and the input image is extracted and retained by Conv, which is called a global feature. The two characteristics are combined as the agent's observation O_t, and then O_t is input into an actor-critic unit composed of two branches. Three fully connected layers (FC) and a long-short-term memory network (LSTM) form the unit. The integrated and combined features of FC are used to obtain high-level meanings, and LSTM is used to remember historical observations. The unit has two output parts, Actor output and Critic output. The former consists of 14-dimensional vectors, corresponding to the probability of taking corresponding actions in the action set, and the latter estimates the expected reward in the current state, which is the state value output. The reward function of the whole process is determined by the difference between the area of the significant area of the cropped image two times before and after and the area of the respective cropped image, which is used to guide the agent to optimize the action. Global and local feature vectors have a dimension of 1000, and FC and LSTM output 1024-dimensional feature vectors.

In summary, in the process of image cropping, the local features obtained by convolution of the cropped image and the global features are combined to provide the observation O_t of current state, and the cropping model provides the Agent with the probability of performing each action in the current state. The Actor output in the Actor-Critic branch instructs the Agent to take corresponding actions, adjust the size and position of the crop window accordingly, and then obtain the final cropped image.

2.4 | Image cropping algorithm description

In the training process of image cropping algorithm, we draw on A3C algorithm.[15] However, unlike the original A3C training algorithm, the asynchronous mechanism is removed during the model training process, and the small batch training
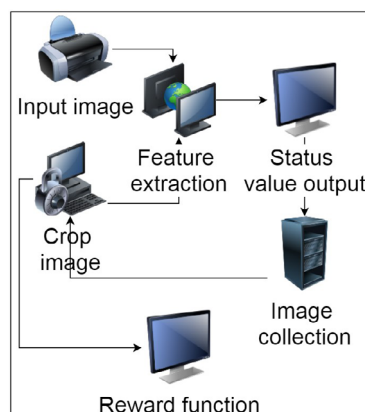

FIGURE 5 Overall structure of the algorithm model.

method is used to increase the diversity of the training process. In the training phase, dominance function and entropy regularization are used as the goal of Actor output optimization. The reward R_t accumulated at step t can be expressed as:

$$R_t = \sum_{i=0}^{k-1} \gamma^i r_{t+i} + \gamma^k V(s_{t+k}, \theta_v) \tag{18}$$

In the formula, γ is the discount factor, r_t is the instant reward obtained at step t, $V(s_{t+k}, \theta_v)$ can represent the value output at state s_t, θ_v represents the Critic branch network parameter, the value range of k is $[0, t_{max}]$, and t_{max} represents the maximum number of update steps.

The optimization goal of Actor output is to maximize the advantage function and output information entropy:

$$y^*_{Actor} = \underset{t}{\arg\max} \{R_t - V(s_t, \theta_v) + H[\pi(s_t, \theta)]\} \tag{19}$$

In the formula, $\pi(s_t, \theta)$ is the actor output probability distribution, θ is the actor branch network parameter, and $H(\cdot)$ is the entropy function, which is used to increase action diversity and enable the agent to obtain flexible action strategies.

The optimization goals of critic output are:

$$y^*_{Critic} = \underset{t}{\arg\min} \frac{1}{2} \cdot [R - V(s_t, \theta_v)]^2 \tag{20}$$

The gradient of the Actor-Critic branch can be expressed as:

$$g_{Actor} = \nabla_\theta \log \pi(a_t|s_t, \theta) \cdot [R - V(s_t, \theta_v)] + \beta \nabla_\theta H[\pi(s_t, \theta)] \tag{21}$$

and,

$$g_{Critic} = \nabla_{\theta_v} \frac{1}{2}[R - V(s_t, \theta_v)]^2 \tag{22}$$

Among them, β is used to control the influence of entropy value, and $\pi(a_t|s_t, \theta)$ is the probability of taking action a_t in state s_t.

2.5 | Description of patients included in the study

The cases in this study are 10 patients with PD who received DBS implantation from June 2018 to June 2019 and are followed up for 1 year. All patients undergo bilateral surgery. Two of them undergo bilateral STN-DBS surgery in our hospital. Among the patients, there are 6 males and 4 females, and the patient's age ranges from 47 to 69 years(mean age:56.2 ± 6.8 years). The course of disease is 4.5–15.5 years(mean course:8.7 ± 3.4 years). The follow-up time is 12–24 months after surgery(mean time:15.1 ± 3.6 months). All patients have end-dose phenomena, and 1 patient has dyskinesia. One patient undergoes globus pallidus operation in the external hospital, and the contralateral symptom is completely relieved.

3 | RESULTS

The root mean square back propagation algorithm (RMSProp) is used to optimize the algorithm model, and the initial learning rate is set to .01 to ensure the fairness of the experiment, and other parameters are set to default values. The batch optimization method is adopted, the number of mini-batch is set to 32, the discount factor γ is set to .99, and the weight of the entropy loss β is set to .05, T_{max} is set to 50, and the update period t_{max} is set to 10. A total of 900 images

are selected from the AVA image database as the verification data set, and the selection method is the same as the training data set. In the entire training process, the Epoch of the training sample times is set to 200, the data set model is verified on each Epoch, and the average effect is reflected as the final model performance.

Then, we conducted experimental tests on two image cropping databases, including the CUHK image cropping database (CUHK-ICD) and the Flickr cropping database (FCD). Moreover, the same metric is used to ensure the fairness of the experiment. The CHUK-ICD database has 950 test images, annotated by three different photographers, and the FCD database contains 348 test images, each of which has only one annotation. In these two databases, this paper selected Intersection over Union (IoU) and Average Displacement (Avg Disp) as evaluation indicators to measure the cutting accuracy of the model. IoU can be defined as follows: If the ground truth window of image i is represented as W_i^g and the crop window is represented as W_i^c, then the average IoU (Avg IoU) of N images can be expressed as:

$$IoU = \frac{1}{N} \cdot \sum_{i=1}^{N} \frac{area(W_i^g \cap W_i^c)}{area(W_i^g \cup W_i^c)} \tag{23}$$

Among them, $area(\cdot)$ represents the area of this area. The average offset represents the average distance between the four edges of the ground truth window and the crop window. In an image, the four edges of the Ground Truth window are defined as $B_i^g(l), B_i^g(r), B_i^g(u)$ and $B_i^g(b)$, respectively, and the four edges of the corresponding crop window are defined as $B_i^c(l), B_i^c(r), B_i^c(u)$, and $B_i^c(b)$, respectively. Then, the average displacement (Avg Disp) in the N images is defined as:

$$AvgDisp = \frac{1}{N} \sum_{i=1}^{N} \sum_{j=\{l,r,u,b\}} \left| B_i^g(j) - B_i^c(j) \right| \cdot \frac{1}{4} \tag{24}$$

We use these two evaluation indicators to measure the performance of the image cropping algorithm. The greater the Avg IoU, and the smaller the Avg Disp, the higher the performance of the algorithm.[16]

Compared with the non-medication state before surgery, the total score of UPDRS III in patients at 6 and 12 months after surgery is significantly decreased in the state of not taking medicine and starting up and the state of taking medicine and starting up (Figure 6), and the difference is statistically significant ($p < .05$). Among them, the improvement rate is the highest in the state of taking medicine and starting up at 12 months after surgery.

However, although the total score of UPDRS III is slightly improved in the state of taking the medicine and starting up at 6 and 12 months after surgery compared with the state of taking the medicine before the surgery, there is no significant difference in the improvement rate ($p > .05$) (Figure 7).
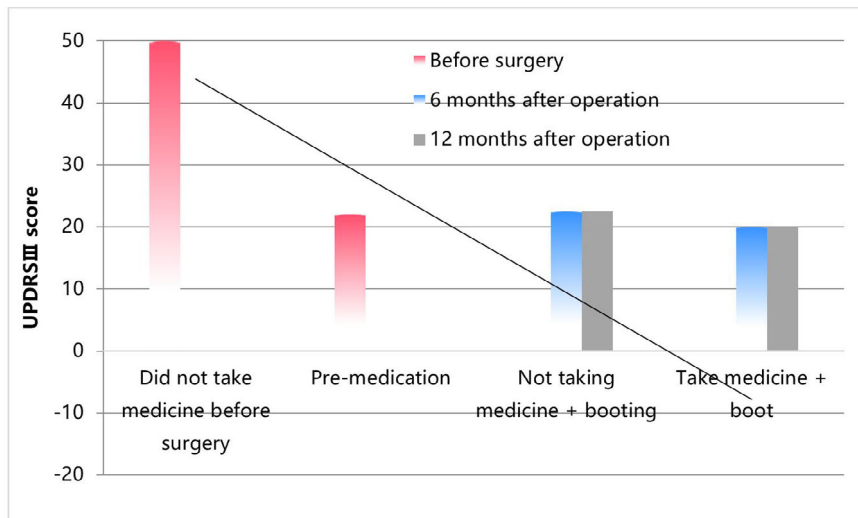

FIGURE 6 Comparison of UPDRS motor status assessment before and after surgery.
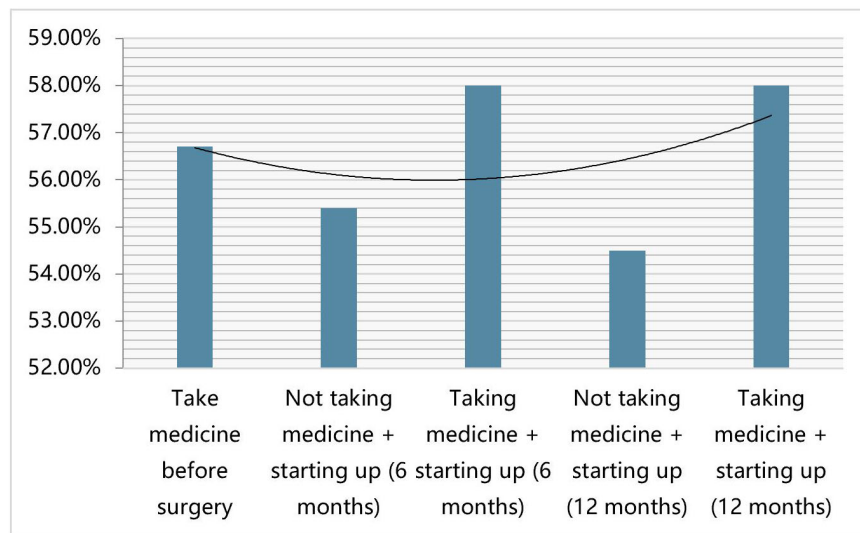
FIGURE 7 Comparison of improvement of motor symptoms before and after surgery.
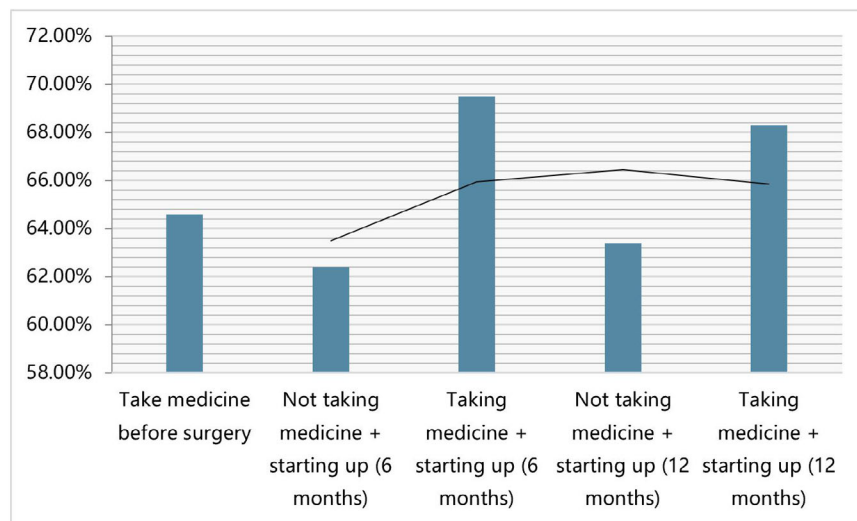

FIGURE 8 Comparison of the improvement of daily life ability before and after surgery.

The scores of the state of not taking the medicine and not starting up at 6 and 12 months after the surgery are slightly increased compared with the state of not taking the medicine before the surgery, but the change is not statistically significant. The quality of life of all patients after surgery is significantly improved. Compared with the state of not taking medicine before surgery, the UPDRSII score improved by 69.3% and 68.4% in the state of taking medicine and starting up at 6 and 12 after surgery, which is significantly improved compared with the state of taking medicine before surgery (Figure 8), the difference is statistically significant ($p < .05$).

The adjustment of the STN-DBS postoperative program-controlled parameters of 10 patients with advanced PD in the order of 6 and 12 months after the surgery is the voltage, frequency and pulse width. None of these parameters increased significantly, and the difference is not statistically significant ($p > .05$) (Table 2). The equivalent dose of levodopa is significantly reduced, but it is related to the dose before surgery. The average daily dose of levodopa in eight PD patients before surgery is 754.0 ± 225.3 mg. However, the average daily equivalent dose of levodopa is reduced to 422.9 ± 115.5 mg and 407.3 ± 114.8 mg in 6 and 12 months after surgery (Figure 9), and the drug reduction rates are 43.8% and 46.9%, respectively. Compared with 6 months after operation, $p > .05$ at 12 months after surgery, the difference is not statistically significant. None of the patients stops taking any levodopa medication.

Through the above analysis, we can see that the method proposed in this study has a certain effect in the detection of PD symptoms after rehabilitation. In actual testing, the model needs to detect a large number of pictures every day. Since the data detected above is less, in order to further verify the performance of the algorithm in this study, a large number of detection pictures are extracted from the hospital database, and the performance of the improved algorithm in this study is verified, and the stability and reliability of the model in this paper under the condition of large data volume are studied, which is convenient for the subsequent clinical application of the model. This article randomly combines the detection images collected from the hospital into 300 sets of data, and each set includes 100 pictures (which can be repeated). The detection accuracy(Accuracy of PD symptoms)and detection speed of the model are verified, and the results shown in Figures 10 and 11 are obtained respectively.

TABLE 2 Comparison table of stimulation parameters at 6 and 12 months after STN-DBS.

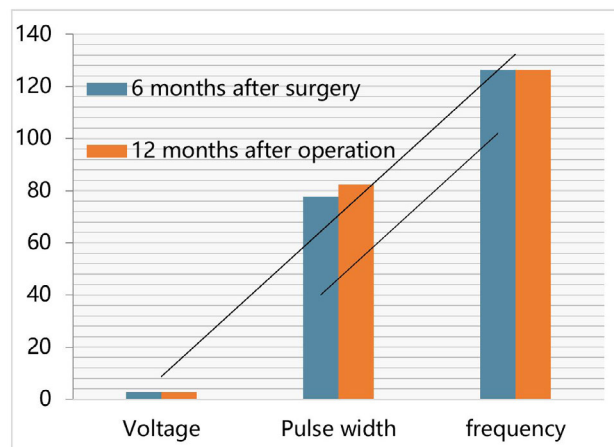| Parameter	n	6 months after surgery	12 months after operation	P value after operation
Voltage	10	$2.7 \pm .2$	$2.8 \pm .2$	$p > .05$
Pulse width	10	77.5 ± 14.9	82.5 ± 11.6	$p > .05$
Frequency	10	126.3 ± 14.1	126.3 ± 7.4	$p > .05$

FIGURE 9 Comparison diagram of stimulation parameters at 6 and 12 months after STN-DBS.
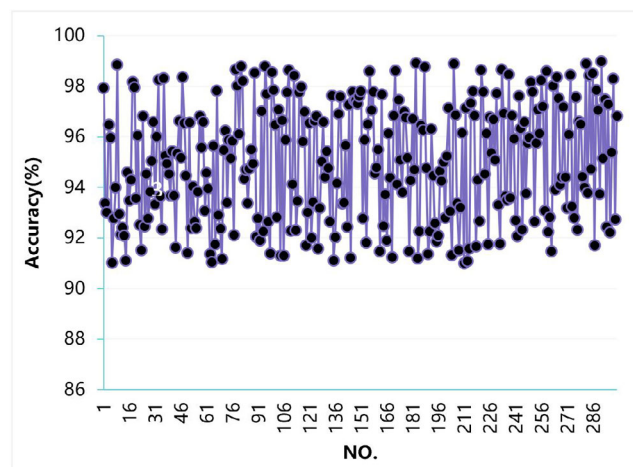

FIGURE 10 Statistical diagram detection accuracy of algorithm model under the condition of big data is between 91% and 99%, with an average of 95%.

It can be seen from Figure 10 that the models constructed in this study have an accuracy rate of more than 90% in the PD detection test, that is, the misdiagnosis rate is less than 10%, which shows that this model has the basis of clinical trials. It can be seen from Figure 11 that the model constructed in this study has a detection time of less than 200 ms for each set of data in PD detection, so it can meet the clinical detection time and needs. Through the analysis of the above detection time and detection accuracy test, it can be seen that the model constructed in this paper meets the current clinical detection needs of PD.

After the stimulator was turned on one month after the operation, all patients' clinical symptoms were significantly improved, and their tremor symptoms were immediately relieved, while the relief of rigidity, bradykinesia, and postural balance disorders were slightly worse. With the long-term stimulation of the stimulator, the amount of anti-PD drugs used by patients has been significantly reduced, and the related complications such as "on–off phenomenon", "end-of-drug phenomenon", and "dyskinetic disorder" caused by long-term large-scale use of anti-PD drugs before surgery have
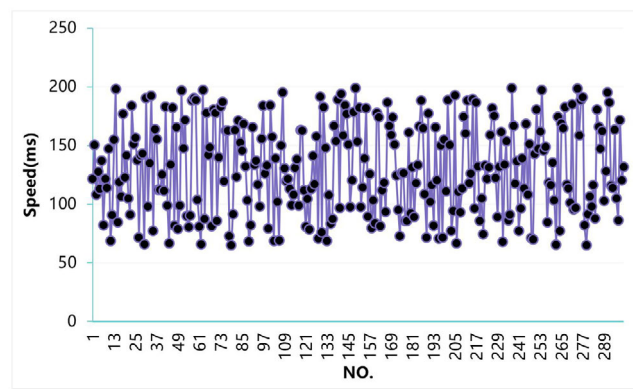

FIGURE 11 Statistical diagram of the detection speed of the algorithm model under the condition of big data is between 60 and 200 ms, with an average of 125 ms.
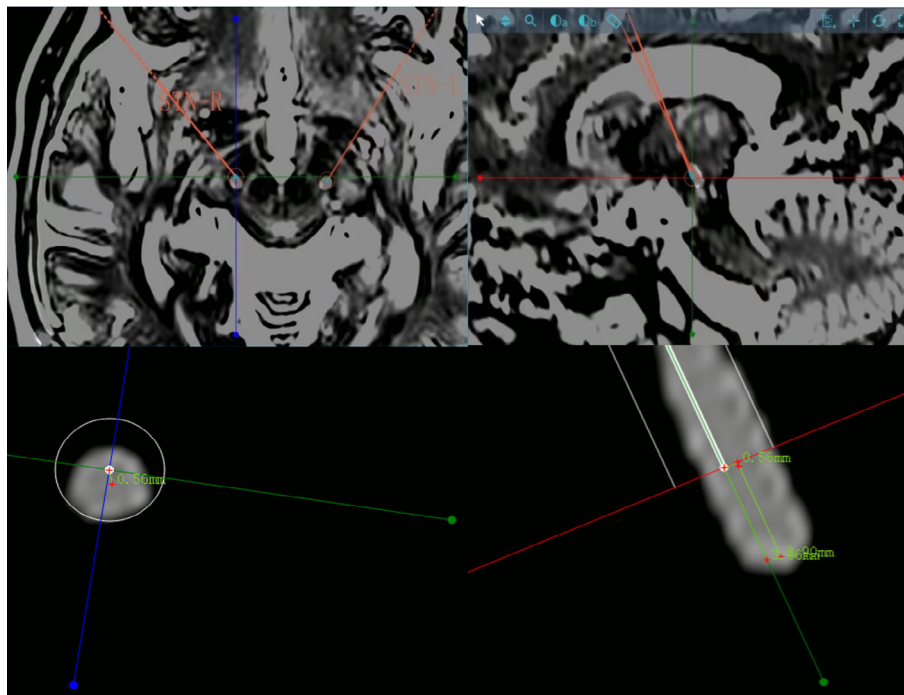

FIGURE 12 Relationship among bilateral electrode position, preoperative planning and STN on MRI. The error between the top of the left electrode and the preoperative plan was .56 mm (axial position), the electrode implantation depth and position are determined according to the electrophysiological signals collected during the operation (sagittal position).

been significantly improved. Moreover, the patient's daily living ability has been significantly improved, and the quality of life has been greatly improved. In addition, patients with STN-DBS treatment had significantly improved motor symptoms and quality of life within 1 year after surgery (Table 1).

we reexamined the cranial CT(128-slice Spiral CT) after DBS and used the Sinovation Plan to reconstruct the electrode. Comparing the error of the implanted electrode tip with the original plan, we found that after using our deep learning algorithm, the error of the electrode was significantly smaller than that of the control group (Figure 12).

4 | DISCUSSION

Since the 1960s, levodopa replacement therapy has been the most effective treatment for PD. However, although levodopa can significantly improve the symptoms of PD patients in the early stage, long-term use of levodopa can cause side effects such as fluctuating symptoms and dyskinesia. Thalamic or globus pallidus surgery can improve the treatment of some drugs with reduced efficacy or intolerable PD, but its use is limited due to surgical trauma and large side effects. DBS implants stimulation electrodes into the target nucleus located in the deep brain tissue of the patient through minimally invasive surgery and sends out weak electrical pulses of a specific frequency through a pulse generator to chronically stimulate the target to achieve the purpose of treatment. Subthalamic nucleus (STN) electrical stimulation therapy has significant clinical effects and low power consumption. Therefore, it is the most commonly used target for DBS treatment of PD. DBS was first clinically applied to treat one patient with advanced PD in 1993. After surgery, the patient's symptoms such as tremor, rigidity, and bradykinesia were significantly improved.[17] In recent years, with the improvement of living standards, many patients with advanced PD have gradually increased their requirements for quality of life. At this time, levodopa's curative effect, end-of-drug phenomenon, and dyskinesia have become the biggest problems for patients.[18] Due to the good therapeutic effect of DBS on patients with advanced PD, it has been widely promoted in clinical treatment. In recent years, the operation has shown a rapid increasing trend. At present, DBS has become one of the most important treatments for patients with advanced PD. According to the results of a recent multicenter study comparing DBS and optimal drug therapy for patients with advanced PD, 70% of patients had significantly improved motor symptoms after DBS, while only 32% of patients who received optimal drug therapy had significantly improved motor symptoms. At the same time, side effects such as symptom fluctuations and dyskinesia in patients after DBS were significantly reduced compared with the best medical treatment, and the quality of life after surgery was significantly improved.[19] The development of DBS has become a milestone in the advanced treatment of PD patients and is also a frontier and hot topic in the field of PD therapy research. Although DBS has a more accurate effect on improving motor symptoms in patients with advanced PD, its effects on non-motor symptoms have been reported differently.[20] Whether DBS can comprehensively improve the motor and non-motor symptoms of PD, whether it is suitable for all patients with PD, and the side effects and other problems that occur after surgery still requires comprehensive clinical observation.[21]

Place a stimulation electrode into the anatomical location means that the effect can be maximized and minimizes side effects. Many factors such as pre-operative planning, intra-operative cerebrospinal fluid loss, and electrode implantation accuracy all affect the outcome. Pre-operative localization of the optimal stimulation zone is the key challenge. Machine learning for producing efficacy probability maps from MRI data appears to be the answer to this challenge.[22] A study contain 187 patients use a patch-based convolutional neural network to classify a stimulation coordinate, proposed classification framework and deep learning method appear well-suited for improving pre-surgical planning and personalize treatment strategies.[23] Stimulated volume modeling and voxel mapping using fast gray matter acquisition T1 inversion recovery (FGATIR) sequences can identify thalamic hypointensity, which can be assessed to predict clinical outcome.[24] In this study, We use a RL algorithm model based on 3.0T MRI image(T1-weighted) analysis technology can effectively help the electrode to reach the target, and obtain better curative effect and less side effects.

PD pathophysiology studies have confirmed that the pathogenesis of the disease is mainly due to degenerative changes of nigra dopaminergic neurons and depletion of striatum dopaminergic transmitters, which leads to excessive enhancement of basal ganglia indirect pathway inhibitory activity and reduction of direct pathway facilitation activity, and ultimately leads to excessive increase of basal ganglia inhibitory output and a series of exercise-reducing symptoms.[25] Although DBS has a significant therapeutic effect and is widely used clinically, the mechanism of action of DBS is still unclear. DeLong et al. believe that DBS mainly uses high-frequency stimulation to suppress excessively excited nuclei in the motor loop of the basal ganglia area and reduce the abnormal output of the basal ganglia to achieve a therapeutic effect.[26] However, during clinical follow-up, it was found that after STN-DBS treatment, the dosage of levodopa can be significantly reduced. Moreover, the therapeutic effect of STN-DBS has a significant correlation with the results of the

preoperative levodopa impact test, suggesting that STN-DBS is related to dopamine. Therefore, many scholars believe that in addition to the electrical stimulation effect, DBS may also promote the secretion or metabolism of dopamine. The literature[27] found that a PD patient with well-controlled symptoms after DBS has acute symptoms worsening after taking fluphenazine, and the efficacy of DBS was completely restored after 4 days of withdrawal. Therefore, from the above situation, it can be seen that blocking the pathway of dopaminergic transmitters can affect the efficacy of DBS, and DBS may play a therapeutic role by participating in the transport mechanism of dopaminergic neurotransmitters. The literature[28] found that DBS can increase the secretion of extracellular dopamine in the striatum of rats with normal or damaged dopaminergic structure through brain microdialysis studies. By using high-performance liquid chromatography (HPLC) technology to detect dopamine transmitters in the striatum of rats after DBS, the literature[29] found that dopamine metabolites such as dihydroxyphenylacetic acid (DOPAC) and homovanillic acid (HVA) increases, which suggests that DBS has a regulatory effect on the dopamine transmitter system. At present, the possible mechanisms of DBS affecting the secretion or metabolism of dopamine transmitters are: ODBS inhibits the substantia nigra (SNr) by inhibiting STN; moreover, SNr and SNc are connected by GABA inhibitory synapses, and weakened SNr activity indirectly increases SNc activity and promotes dopamine secretion. DBS can enhance the effect of STN on glutamatergic excitability of SNc dopaminergic neurons.[30] DBS can produce both inhibition and excitement for STN. On the one hand, electrical stimulation inhibits STN activity, and on the other hand, it stimulates the axons (even cell bodies) connected to STN neurons. STN can stimulate STN to contact the glutamate synaptic connection of SNc dopaminergic neurons during electrical stimulation, increase the frequency of SNc dopaminergic neurons, and promote dopamine secretion. However, some studies have reached the opposite conclusion, and studies believe that DBS does not affect the change of dopaminergic transmitters.[31] The literature[32] and the literature[33] used Raclopride PET to follow up PD patients after DBS. The study found that although postoperative motor symptoms are significantly improved, no significant changes in dopamine receptor binding rate are found. Therefore, the study speculated that DBS cannot increase the level of dopamine transmitters in the striatum. The literature[34] believed that the subjects of the above clinical studies are all patients with advanced PD who have a longer course of disease, and the patient's substantia nigra system has undergone severe degenerative changes. Therefore, the response of dopamine receptors to dopamine is relatively poor, and it is inaccurate to use the changes in dopamine receptor binding rate in these patient populations to indirectly reflect the changes of dopamine transmitters in the substantia nigra.

5 | CONCLUSION

Patients with PD are mainly clinically characterized by bradykinesia, tremor, and rigidity, which seriously affect the patient's activities, emotions and life and cause the patient's quality of life to decline. Due to its unique advantages and good curative effect, DBS has almost replaced damage surgery as the mainstream of PD surgical treatment in the world. Based on the deep learning algorithm, this study combines with MRI image analysis technology to study the clinical efficacy of DBS in the surgical treatment of PD, and to study its neuroprotective and neural recovery effects after surgery. Moreover, this study improves the deep learning algorithm so that it can be combined with clinical imaging to construct a corresponding imaging analysis model. Through the analysis of experimental research, it can be seen that DBS can significantly improve a series of clinical symptoms such as tremor, rigidity, and bradykinesia in patients with PD, improve the quality of life of patients, significantly reduce the amount of anti-PD drugs used after surgery, and alleviate the side effects caused by excessive drug consumption. Therefore, DBS is the first choice for the treatment of patients with advanced PD.

CONFLICT OF INTEREST
The authors declare no conflicts of interest.

DATA AVAILABILITY STATEMENT
The data that support the findings of this study are available from the corresponding author upon reasonable request.

ORCID
Xiang Xiao https://orcid.org/0000-0002-3060-0299

REFERENCES

1. Lhommée E, Batir A, Quesada JL, et al. Dopamine and the biology of creativity: lessons from Parkinson's disease. *Front Neurol.* 2014; 5:55.

2. Mitchell KT, Ostrem JL. Surgical treatment of parkinson disease. *Neurol Clin.* 2020;38(2):293-307.

3. Benoit CE, Dalla Bella S, Farrugia N, et al. Musically cued gait-training improves both perceptual and motor timing in Parkinson's disease. *Front Hum Neurosci.* 2014;8:494.

4. Rietdijk CD, Perez-Pardo P, Garssen J, Van Wezel RJA, Kraneveld AD. Exploring Braak's hypothesis of Parkinson's disease. *Front Neurol.* 2017;8:37.

5. Lord S, Galna B, Coleman S, et al. Cognition and gait show a selective pattern of association dominated by phenotype in incident Parkinson's disease. *Front Aging Neurosci.* 2014;6:249.

6. Ashoori A, Eagleman DM, Jankovic J. Effects of auditory rhythm and music on gait disturbances in Parkinson's disease. *Front Neurol.* 2015;6:234.

7. Ridgel AL, Phillips RS, Walter BL, Discenzo FM, Loparo KA. Dynamic high-cadence cycling improves motor symptoms in Parkinson's disease. *Front Neurol.* 2015;6:194.

8. Pau M, Corona F, Pili R, et al. Effects of physical rehabilitation integrated with rhythmic auditory stimulation on spatio-temporal and kinematic parameters of gait in Parkinson's disease. *Front Neurol.* 2016;7:126.

9. di Biase L, Summa S, Tosi J, et al. Quantitative analysis of bradykinesia and rigidity in Parkinson's disease. *Front Neurol.* 2018;9:121.

10. Procházka A, Vyšata O, Vališ M, Ťupa O, Schätz M, Mařík V. Bayesian classification and analysis of gait disorders using image and depth sensors of Microsoft Kinect. *Digit Signal Process.* 2015;47:169-177.

11. Sandoval-Rincón M, Sáenz-Farret M, Miguel-Puga A, et al. Rational pharmacological approaches for cognitive dysfunction and depression in Parkinson's disease. *Front Neurol.* 2015;6:71.

12. Salvatore C, Cerasa A, Castiglioni I, et al. Machine learning on brain MRI data for differential diagnosis of Parkinson's disease and progressive supranuclear palsy. *J Neurosci Methods.* 2014;222:230-237.

13. Camalier CR, Konrad PE, Kao CC, et al. Methods for surgical targeting of the STN in early-stage Parkinson's disease. *Front Neurol.* 2014; 5:25.

14. Kumar J, Eraña H, López-Martínez E, et al. Detection of amyloid fibrils in Parkinson's disease using plasmonic chirality. *Proc Natl Acad Sci.* 2018;115(13):3225-3230.

15. Pham MH, Elshehabi M, Haertner L, et al. Validation of a step detection algorithm during straight walking and turning in patients with Parkinson's disease and older adults using an inertial measurement unit at the lower back. *Front Neurol.* 2017;8:457.

16. Zheng Z, Shemmassian S, Wijekoon C, Kim W, Bookheimer SY, Pouratian N. DTI correlates of distinct cognitive impairments in Parkinson's disease. *Hum Brain Mapp.* 2014;35(4):1325-1333.

17. Chen Y, Storrs J, Tan L, Mazlack LJ, Lee JH, Lu LJ. Detecting brain structural changes as biomarker from magnetic resonance images using a local feature based SVM approach. *J Neurosci Methods.* 2014;221:22-31.

18. Gonzalez-Redondo R, García-García D, Clavero P, et al. Grey matter hypometabolism and atrophy in Parkinson's disease with cognitive impairment: a two-step process. *Brain.* 2014;137(8):2356-2367.

19. Torres F, Villalon E, Poblete P, et al. Retrospective evaluation of deep transcranial magnetic stimulation as add-on treatment for Parkinson's Disease. *Front Neurol.* 2015;6:210.

20. Skodda S, Grönheit W, Schlegel U, Südmeyer M, Schnitzler A, Wojtecki L. Effect of subthalamic stimulation on voice and speech in Parkinson's disease: for the better or worse? *Front Neurol.* 2014;4:218.

21. Guan X, Xuan M, Gu Q, et al. Regionally progressive accumulation of iron in Parkinson's disease as measured by quantitative susceptibility mapping. *NMR Biomed.* 2017;30(4):e3489.

22. Watts J, Khojandi A, Shylo O, Ramdhani RA. Machine learning's application in deep brain stimulation for Parkinson's disease: a review. *Brain Sci.* 2020;10(11):809.

23. Bermudez C, Rodriguez W, Huo Y, et al. Towards machine learning prediction of deep brain stimulation (DBS) intra-operative efficacy maps. *Proc SPIE Int Soc Opt Eng.* 2019;3:10949.

24. Neudorfer C, Kroneberg D, Al-Fatly B, et al. Personalizing deep brain stimulation using advanced imaging sequences. *Ann Neurol.* 2022; 91(5):613-628.

25. Reimao S, Pita Lobo P, Neutel D, et al. Substantia nigra neuromelanin magnetic resonance imaging in de novo Parkinson's disease patients. *Eur J Neurol.* 2015;22(3):540-546.

26. Agrawal R, Ahuja K, Hoo CH, Nguyen TDA, Kumar A. ParaLarPD: Parallel FPGA router using primal-dual sub-gradient method. *Electronics MDPI.* 2019;8(12):1439.

27. Ginis P, Heremans E, Ferrari A, Dockx K, Canning CG, Nieuwboer A. Prolonged walking with a wearable system providing intelligent auditory input in people with Parkinson's disease. *Front Neurol.* 2017;8:128.

28. La Morgia C, Ross-Cisneros FN, Sadun AA, et al. Retinal ganglion cells and circadian rhythms in Alzheimer's disease, Parkinson's disease, and beyond. *Front Neurol.* 2017;8:162.

29. Sérrière S, Doméné A, Vercouillie J, et al. Assessment of the protection of dopaminergic neurons by an α7 nicotinic receptor agonist, PHA 543613 using [18F] LBT-999 in a Parkinson's disease rat model. *Front Med.* 2015;2:61.

30. Zhang D, Liu X, Chen J, Liu B, Wang J. Widespread increase of functional connectivity in Parkinson's disease with tremor: a resting-state FMRI study. *Front Aging Neurosci.* 2015;7:6.

31. Mnih V, Kavukcuoglu K, Silver D, et al. Human-level control through deep reinforcement learning. *Nature*. 2015;518(7540):529-533.

32. Chen D, Chu H. Scale-invariant amplitude spectrum modulation for visual saliency detection. *IEEE Trans Neural Netw Learn Syst*. 2012; 23(8):1206-1214.

33. Wei Q, Wang L, Liu Y, Polycarpou MM. Optimal elevator group control via deep asynchronous actor-critic learning. *IEEE Trans Neural Netw Learn Syst*. 2020;31(12):5245-5256.

34. Park SC, Cha JH, Lee S, Jang W, Lee CS, Lee JK. Deep learning-based deep brain stimulation targeting and clinical applications. *Front Neurosci*. 2019;13:1128.